## A NEW VERSATILE, LARGE SIZE MOVPE REACTOR

## P.M. FRIJLINK

Laboratoires d'Electronique et the Physique Appliquée (LEP) \*, 3 Avenue Descartes, F-94451 Limeil-Brévannes Cedex, France

A new reactor for MOVPE of III-V semiconductors is presented. Seven 2 inch wafers or five 3 inch wafers are in planetary motion in a circular growth chamber, with the gas flowing radially from the centre to the edge. The planetary motion is achieved using a new technique of levitation and rotation of the substrate holder, which is described in detail. The chamber geometry is also described in detail, and numerical mass transport simulations are compared with experimental results on growth at atmospheric pressure. Thickness and doping of GaAs layers are uniform to within  $\pm 1\%$  on 2 inch wafers. GaAs-Ga<sub>0.5</sub>Al<sub>0.5</sub>As quantum well photoluminescence spectra are shown. Very high mobilities obtained on GaAs-(Ga,Al)As two-dimensional electron gas structures with a record value of 720,000 cm<sup>2</sup>/ $\bar{V}$ s at 1.5 K are reported.

### 1. Introduction

The MOVPE technique has now come into a phase where it should be considered as a reliable step in many of the processes to make III-V devices. Research on a new device process usually requires to restart the whole processing sequence many times, each time to optimize one further process step, until finally the end-product works correctly. Optimization of a process step is often done by variation of one process parameter, while all the other parameters, including those of the epitaxial layer structure should remain constant. It is clear that at each restart of the processing sequence, it could be quite useful to start with a small series of wafers with perfectly identical epitaxial layers. The ideal MOVPE reactor should therefore be able to simultaneously grow uniform and strictly identical layers on several wafers. However, uniformity, electrical and optical layer quality should be at least equal to those obtainable with single wafer reactors.

This paper introduces an MOVPE reactor in which seven two inch wafers are put in a circle on a horizontal round table turning around its central axis. Each wafer is also turning around its own axis. The reactive gases enter just above the centre

of the table and flow radially outwards between the table and a horizontal quartz plate. The main rotation of the table and its sevenfold symmetry provide a perfect exchange of the wafer positions and guarantee, by principle, a high degree of equality of the simultaneously grown epilayers.

## 2. General concept

A simplified, schematic cross-section of the reactor chamber is shown in fig. 1. The graphite substrate support has the outline of a disk of diameter 246 mm and thickness 28 mm. It consists of a base (1), a main platform (2) which turns around a main central axis and - in the two inch version - seven satellite plateaus (3), each one supporting a wafer (4) and each one turning around its axis at a distance of 80 mm from the central axis. The main platform has a seven-fold rotational symmetry. The satellites have an infinite rotational symmetry. The main platform as well as the satellite platforms are supported by a gas foil, which also provides the rotation. The rotation speeds of the main platform and of the satellites are controlled separately by two distinct hydrogen flows.

The substrate support is placed between two quartz disks, inside a perforated quartz ring (5)

0022-0248/88/\$03.50 © Elsevier Science Publishers B.V. (North-Holland Physics Publishing Division)

<sup>\*</sup> A member of the Philips Research Organization.

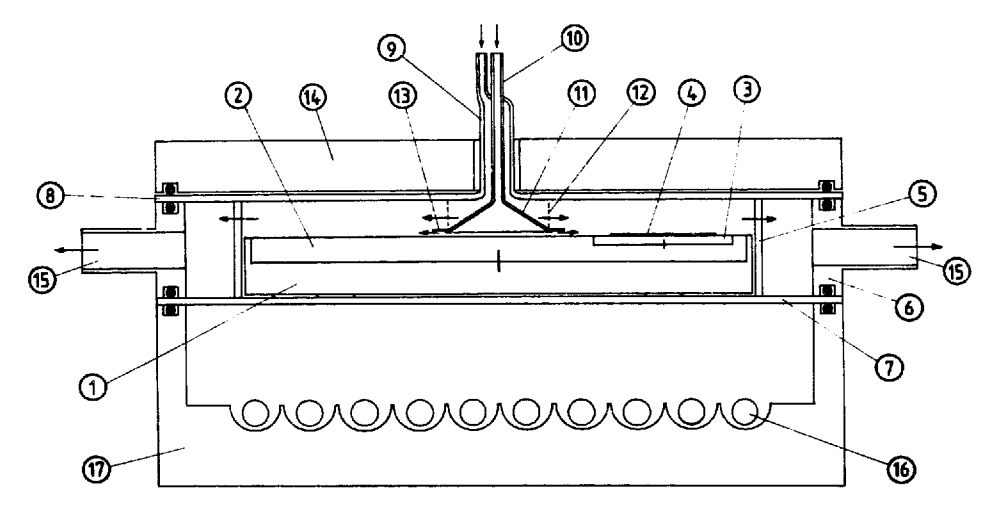


Fig. 1. Cross-section of the reactor chamber through the main axis. The numbers refer to the text. The reactive gas flow is indicated by arrows.

and a water cooled stainless steel ring (6). The two quartz disks and the stainless steel ring form the outer limitation of the hydrogen atmosphere of the growth chamber. The lower quartz disk (7) supports the substrate holder. The upper quartz disk (8) has a central hole with two coaxial tubes attached to it. The main hydrogen carrier flow, the group III organometallics and the dopants enter through the outer tube (9). The second hydrogen carrier flow and group V hydride flows enter through the inner tube (10), which ends in a cone (11). The narrow slit between the substrate holder and the cone provides an equal distribution in the growth chamber of group V species over all radial directions.

In general, if a stable and uniform radial gasflow pattern must be established, in a space with a ring-form, with inner diameter  $R_1$  and outer diameter  $R_2$ , the ratio  $R_2/R_1$  should not be too large because otherwise stationary horizontal vortices will form with their axis perpendicular to the plane of the ring, and the bulk of the flow passes in one or more corridors between the vortices. In an early version of the design, this parasitic behaviour has indeed been observed. To avoid it, the group III species and the main carrier enter the inner growth chamber through a cylindric entrance grating (12), placed between the edge of the cone and the upper quartz plate. This molybdenum piece contains 17 equal slits, from which the gas flows tangentially into the inner growth chamber, providing a uniform stable radial distribution of the gases in the growth chamber and effectively suppressing – even at 1 atm – all horizontal vortices in the growth chamber for the used practical flow rates.

The III and V products are initially separated by a molybdenum deflector ring (13) which brings III and V flows in contact only after the entrance jet effects of the III flow and main carrier have sufficiently diminished, and the main carrier is sufficiently heated. In this way, the group V flow will smoothly follow the surface of the substrate holder, and always keep sufficient group V excess pressure on the wafers, and provide by its mass an increased stability against thermal convection between the hot (700°C) substrate holder and the colder (400°C) quartz ceiling plate. The distance between the substrate holder and the ceiling is 15 mm.

The temperature of the ceiling plate can be controlled between about 300 and  $500\,^{\circ}$ C by adjusting the  $H_2$  content in the  $H_2/Ar$  mixture in the slit between the water-cooled aluminium top plate (14) and the quartz ceiling plate (8). The width of the slit is about 0.5 mm. Inside such a narrow slit, convective flow does not occur because the product of the Grashof and Prandl numbers is very much smaller than 1000. The main heat transport mechanism across the slit will be by conduction of the gas. The thermal conductivity of  $H_2$  is about ten times the conductivity of

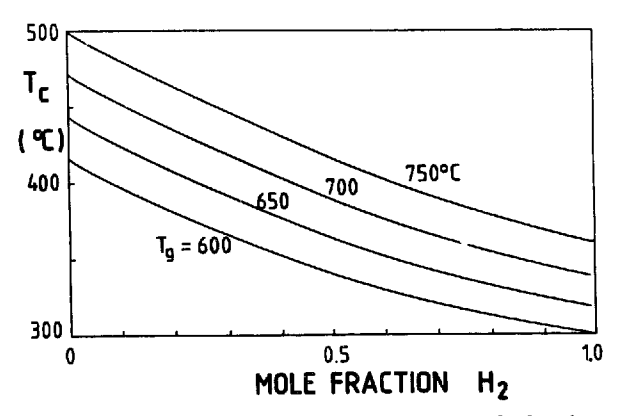


Fig. 2. Calculated ceiling temperature versus mole fraction of  $H_2$  in the  $Ar-H_2$  mixture in the slit between quartz ceiling plate and cooled top plate, for several growth temperatures. The temperature of the top plate is assumed 50 ° C. The width of the slit is 0.5 mm.

argon. Fig. 2 shows the calculated dependence of the ceiling temperature on the composition of the gas mixture, assuming that the heat transport between substrate holder and ceiling is by radiation only and not by convection.

This temperature is adjusted at about 400°C to avoid deposition of arsenic, phosphorus, or solid hydrogen phosphides occurring at lower temperatures, and also to limit III-V growth by kinetic limitation. In practice, deposit at an intermediate temperature on a quartz surface is avoided only if the gas did not previously pass a section at high temperature, because otherwise - i.e. in the case of GaAs growth - a thick granulous deposit will occur. In this reactor, this deposit does not occur on the ceiling and the GaAs thickness on the ceiling is of the order of 1% of the thickness of the epitaxial layer on the wafers, thus indicating the absence of convective flow. The general problem of loosened ceiling deposit falling on the wafers, occurring in horizontal reactors, which necessitates frequent cleaning, is solved in this way.

After flowing radially through the inner growth chamber, the gases flow through the perforated quartz ring (5) into the collector space between the quartz ring and stainless steel ring (6). From this space, two tubes at diametrically opposite sides (15) lead to the exhaust gas treatment. The pressure drop over (5) is much larger than the pressure drop in the collector space, thus assuring a radial flow distribution in the inner growth chamber.

The graphite substrate holder is heated by 10 infrared tube lamps (16) of 2 kW each, with a water cooled high efficiency elliptic reflector (17) with focal points on the susceptor. By separately addressing each lamp, the temperature distribution of the base plate (1) is uniformized.

## 3. Gas foil rotation

Fig. 3 shows the basic principle. A disk with a small axis hole in its lower flat surface covers another disk with three shallow spiral grooves in its upper flat surface. Each spiral groove has a small hole in its end near the center of the disk, out of which a gas flows, coming from below.

The lower disk also has a small hole in the centre of its upper surface in which an axis is fitted, which centers the upper disk, but does not support it. The gas flowing out of the three holes is going to lift the upper disk, and is preferentially, but no exclusively, following the spirals. Because of the narrow spacing between the disks, the flow between the two surfaces is in all cases a perfectly laminar viscous flow with a parabolic velocity profile. With well-designed spiral grooves, the upper disk is lifted by the gas flow providing a uniform slit between the two disks and the viscous shear force of the gas flow along the spiral grooves makes the upper disk turn.

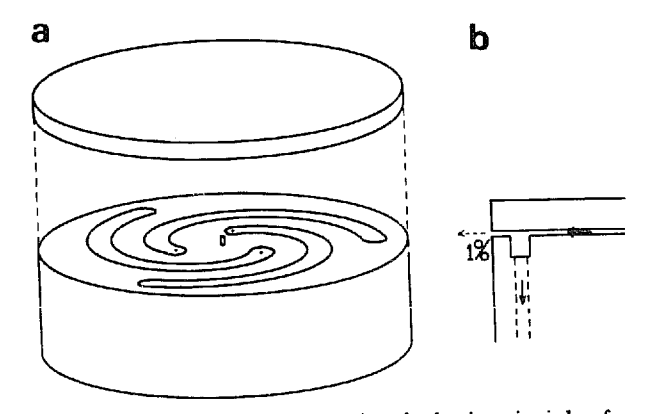


Fig. 3. Schematic drawing, indicating the basic principle of gas foil rotation by an exploded view. The upper disk is rotated and levitated by the gas flowing out of the three holes in the lower disk. The small axis only centers but does not support. The normal distance between the surfaces of the two disks is  $50-100 \ \mu m$ .

To optimize the geometry of the spirals, a computer program was made to calculate the flow distribution between the two disks by a two dimensional Green function method [1]. The contours of the spiral and of the disk are approximated by line segments. For a given height of flight of the upper disk, the program optimizes the flow to a value such that the integral over the resulting pressure distribution is equal to the gravitational force on the upper disk. For a given spiral geometry, fig. 4 shows the torque versus hydrogen flow for different spiral groove depths and, for one flow and one spiral depth, fig. 5 shows the pressure distribution. Fig. 4 also shows the experimental torque measured on a real graphite substrate holder with this geometry, for different hydrogen flows, by timing the first few rotations after the start of the flow, and by measuring the final steady state rotation speed, which is given by an equilibrium between the friction torque of the axis and the torque of the gas flow. The agreement for H<sub>2</sub> is good. The slight difference may be explained by the fact that the mass of the gas, which makes it more difficult for the gas to leave the spiral groove, was not taken into acount. If the mass of the gas is neglected, then the viscosity and the volumetric flow do not enter separately into the equations, but only their product. This explains that, experimentally, at 700 °C, about 5 times less H<sub>2</sub> mass flow is needed than at

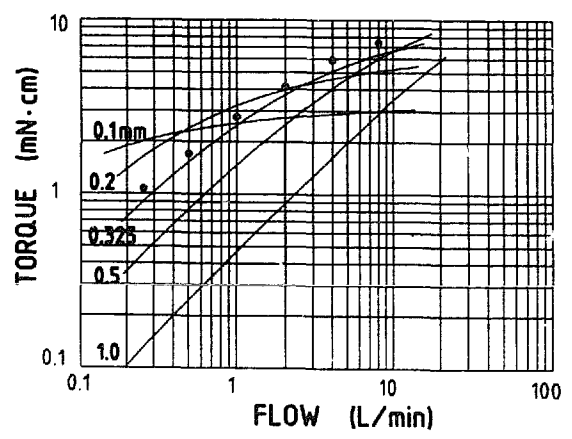


Fig. 4. Calculated and experimental torque versus hydrogen flow at 300 K for the spiral geometry of fig. 5, for several spire depths. The weight of the upper disk is 1.643 g/cm<sup>2</sup>. The points indicate measured values for a spire depth of 0.325 mm. Ambient pressure is 1 atm.

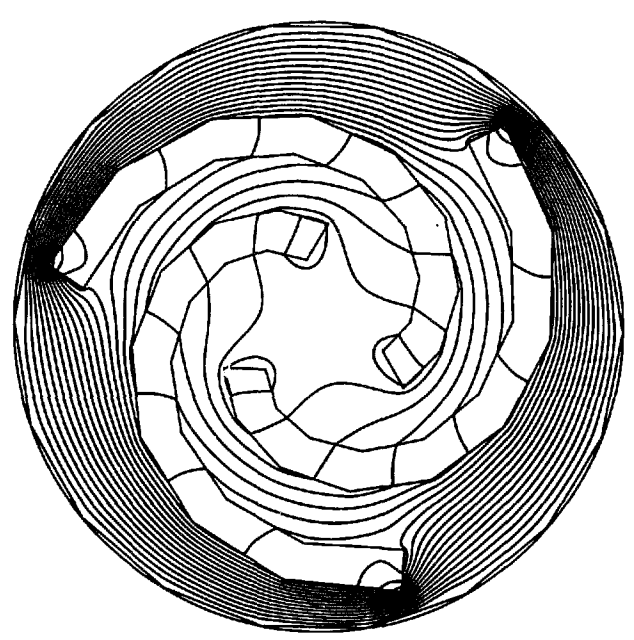


Fig. 5. Calculated pressure distribution indicated by the isobar pattern. The pressure difference between isobars is normalized to 1/20 of the maximum overpressure. The overall diameter is 58 mm. The weight of the upper disk is 1.643 g/cm<sup>2</sup>. The spire depth of 0.325 mm. The flow is 909 cm<sup>3</sup>/min. The distance between the surfaces of the two disks is 70 μm.

room temperature, and at 0.1 bar about 10 times less than at 1 bar, to obtain the same rotation speed.

The thickness of the gas-foil between the satellite platforms and the main turning platform is about 50  $\mu$ m. At a growth temperature of 700 °C, when the satellite disk emits about 5 W/cm² of heat radiation from its upper surface, the temperature difference over the gas foil will be 6 °C.

The extension of the principle to a planetary motion with a main platform and any number of satellite platforms is straightforward. In the substrate holder, used in this reactor, the gas flows used for the rotation do not flow out into the reactor chamber as in fig. 3a, but they are collected in a circular groove surrounding the spirals, as in fig. 3b, and flow out below the base (1). Only about 1% of the gas is flowing into the inner growth chamber. At 700°C and 1 atm, the flow used for the main disk is 1 SLM for a rotation speed of about 0.5 cycles/s and the total flow on the seven satellites is also 1 SLM for for a rotation speed of about 3 cycles/s. This means that the

rotation gas flowing into the inner growth chamber upstream of each wafer represents about 0.7 SCCM.

## 4. Simulation of heat and mass transport

The present numerical simulation is based on a laminar flow model, of which the details and the experimental verification are published elsewhere [2]. The essential features are that:

- For GaAs growth from TMG and AsH<sub>3</sub>, one mean diffusion coefficient may be used for Ga species, of value 0.397  $(T/300)^{1.67}$  for T < 850 K, 0.484  $(T/300)^{1.67}$  for T > 950 K, and a linear interpolation between those functions for 850 < T < 950 K. For As species, D = 0.55  $(T/300)^{1.67}$ .
- Horizontal transport of reactive species is supposed only by flow. Horizontal diffusion is neglected.
- The reactive species follow the streamlines, and vertical re-distribution between the streamlines is by diffusion.
- The inertial forces due to the mass of the gas are taken into account, including the contribution to the mass of group V species.
- The total pressure  $P_{\text{tot}}$  of the gas is only a function of radius r.
- From ref. [2], it was found that the concentration of Ga and Al bearing species in the gas in the direct vicinity of the surface is smaller than 10<sup>-7</sup> bar for the range of growth temperature and growth rates used in this paper. This concentration was therefore approximated by zero: the growth rate is only determined by mass transport. A difference in surface roughness between the wafer surface and the surrounding graphite will not influence the mass transport pattern in the gas.

In this case, at atmospheric pressure, it is believed that the initial 17 tangential entrance jets of the first carrier and the flow of the second carrier combine within a centimetre or so from the entrance (at R=36 mm) to an almost purely radial velocity profile (between substrate holder and ceiling plate). Experimentally, convective flow is absent. Although it is only an approximation, the simulation greatly helps understanding of how a

uniform thickness profile on the wafers is obtained and what parameters influence the thickness profile on the wafer and to what extent.

To give a summary of the equation used:

flow density J of reactive species

$$\mathbf{J} = \mathbf{v}C - G \text{ grad } C/C_{\text{tot}}, \tag{1}$$

with mass transfer coefficient

$$G = (P_{\text{tot}}/R_{g}T)D, \tag{2}$$

continuity equation of reactive species

$$\partial C/\partial t = -\operatorname{div} \mathbf{J} = 0$$
 in steady state, (3)

continuity equation of the carrier gas

$$\operatorname{div}(C_{\operatorname{tot}}v) = 0, \tag{4}$$

hence

$$\mathbf{v} \cdot \operatorname{grad} C = \frac{C}{C_{\text{tot}}} \mathbf{v} \cdot \operatorname{grad} C_{\text{tot}} + \operatorname{div} \left( G \operatorname{grad} \frac{C}{C_{\text{tot}}} \right),$$
(5)

partial pressure

$$P = (C/C_{\text{tot}})P_{\text{tot}}. (6)$$

Hence, neglecting the variation of  $P_{tot}$ ,

$$C_{\text{tot}} v \cdot \text{grad } P = \text{div}(G \text{ grad } P).$$
 (7)

In polar coordinates radius r, and  $\varphi$  and vertical coordinate y:

supposing 
$$v_{\varphi} = 0$$
,  $v_{\nu} \approx 0$ , (8a)

$$\frac{1}{r}\frac{\partial}{\partial r}\left(rG\frac{\partial P}{\partial r}\right) \ll \frac{\partial}{\partial \nu}\left(G\frac{\partial P}{\partial \nu}\right),\tag{8b}$$

$$\frac{\partial P}{\partial \varphi} = 0. \tag{8c}$$

These equations simplify to

$$C_{\text{tot}} v_r \frac{\partial P}{\partial r} = \frac{\partial}{\partial y} \left( G \frac{\partial P}{\partial y} \right). \tag{9}$$

Similarly, for heat transport,

$$c_{p}C_{\text{tot}}v_{r}\frac{\partial T}{\partial r} = \frac{\partial}{\partial y}\left(k\frac{\partial T}{\partial y}\right). \tag{10}$$

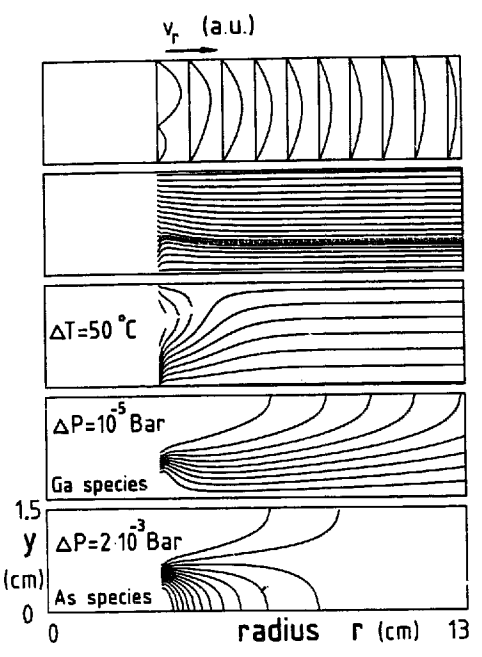


Fig. 6. Calculated vertical cross-sectional maps of the growth chamber for growth at 700 °C, with the ceiling at 400 °C: (a) velocity profiles; (b) streamline patterns; (c) isotherms ( $\Delta T = 50$  °C); (d) isobars of partial pressure of Ga bearing species ( $\Delta p = 10^{-5}$  bar); (e) isobars of partial pressure of As bearing species ( $\Delta p = 2 \times 10^{-3}$  bar).

The velocity field is determined by

$$\frac{\mathrm{d}P_{\mathrm{tot}}}{\mathrm{d}r} = \eta \frac{\partial^2 v_r}{\partial y^2} - \rho \frac{\partial v_r}{\partial r} v_r. \tag{11}$$

These equations are numerically solved by a straightforward finite difference method. Fig. 6 shows the resulting mappings of the velocity profile, streamline pattern, isotherms and isobars.

Fig. 7 shows the growth rate profiles  $\tau(R)$  of the deposit on the substrate holder for two different sets of carrier flows. To obtain the growth rate profile  $\tau^*(r)$  on a rotating wafer with axis centred at  $R_b = 80$  mm from the central axis, we have to do the transformation:

$$\tau^*(r) = \lim_{n \to \infty} \frac{1}{n} \sum_{i=1}^n \tau \left( \left[ \left( R_b + r \cos \frac{2\pi i}{n} \right)^2 + \left( r \sin \frac{2\pi i}{n} \right)^2 \right]^{1/2} \right). \tag{12}$$

Fig. 8 shows the resulting calculated growth rate profiles on the wafer for the conditions of fig.

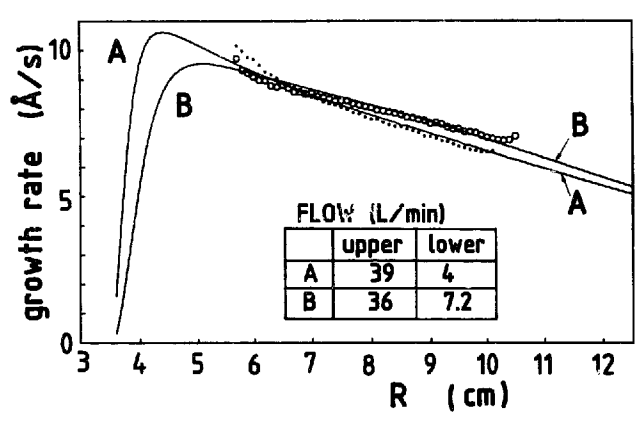


Fig. 7. Calculated (solid lines) and experimental (points) growth rate profiles of the deposit on the substrate holder for two different sets of carrier flows. The temperature of the substrate holder is 700 °C, the ceiling 400 °C, and the injection temperature of the gas is 300 °C.

7 with rotating satellites. Note that the profiles in fig. 8 are both convex, while one of the profiles in fig. 7 is clearly concave near  $R_b = 80$  mm. The reason is the during rotation, a point on the edge of the wafer is a somewhat longer time outside the circle with radius  $R_b$  than it is inside it. To obtain a perfectly uniform profile  $\tau^*(r)$  from a monotonically descending profile  $\tau(R)$ , this profile must be slightly concave.

### 5. Experimental results

The reactor chamber was mounted inside a glove-box. A conventional gas cabinet was used to provide the necessary carrier gas flows, reactant flows and rotation flows. For GaAs and (Ga,Al)As

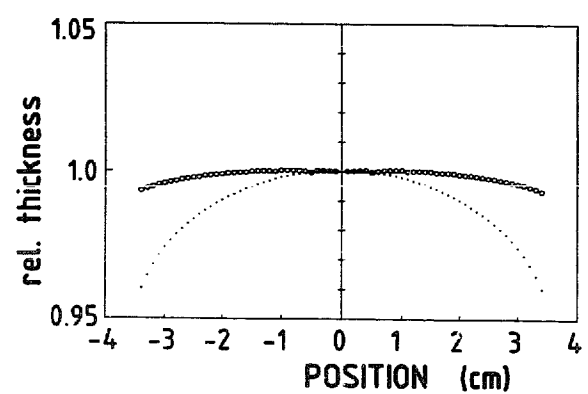


Fig. 8. Calculated normalized thickness profiles on the rotating wafer for curve A (circles) and curve B (dots) of fig. 7.

growth, trimethylgallium, arsine, trimethylaluminium were used. Si<sub>2</sub>H<sub>6</sub> was used as n-dopant.

# 5.1. Uniformity

To measure the uniformity of the deposit, an epitaxial layer structure consisting of an n-doped GaAs layer on top of a (Ga,Al)As layer was grown. The (Ga,Al)As layer was grown during 5 min with a TMG flow of 20 cm³/min at 68 mbar, and a TMA flow of 200 cm³/min at 8 mbar. The GaAs layer was grown during 40 min with a TMG flow of 50 cm³/min at partial pressure of 68 mbar and doped with 40 cm³/min of 50 ppm Si<sub>2</sub>H<sub>6</sub> in H<sub>2</sub>. The arsine flow was 200 cm³/min and the total carrier flow 43 1/min. The growth temperature was 700°C. The obtained surface is with and without magnification totally smooth and aspectless.

For measurement of the thickness uniformity, one half of the wafer was masked with wax, after which the wafer was exposed to a solution of 200 cm<sup>3</sup>  $H_2O_2$  30% in  $H_2O + 10$  cm<sup>3</sup> citric acid 200 g/l + sufficient NH<sub>4</sub>OH to obtain pH = 8. The used etch rate of GaAs, very dependent on the pH was about 6  $\mu$ m/h. This etch totally blocks on (Ga,Al)As with more than 40% Al. After removing the wax, the thickness profile was determined by measuring the step using a moving stylus apparatus.

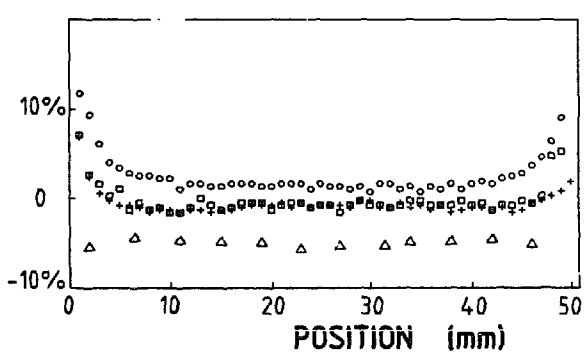


Fig. 9. Measured uniformity with rotating satellites. Deviation with respect to an arbitrary reference value versus position on wafer. Crosses and squares: thickness on two wafers of the same run with growth conditions corresponding to fig. 7 curve B. Triangles: sheet resistivity on one of these wafers. Circles: thickness on one wafer with growth condition corresponding to fig. 7 curve A. The reference value of this curve has been shifted for clarity of the figure.

For measurement of the doping uniformity, a narrow bar was cleaved through the diameter of the wafer, from which many clover shaped samples were made, on which the sheet resistance could be measured precisely. Fig. 7 shows a comparison between calculated and experimental thickness profiles on a 2 inch wafer when only the main plateau was rotated. Fig. 9 is a relative plot of the resulting thickness profiles and sheet resistance when also the satellites were rotating.

In both fig. 7 and fig. 9, we clearly see an edge effect: the thickness increases rapidly towards the edge of the wafer. This effect is due to the protuberance of the edge of the wafer, which makes it collect more of the diffusing reactant per unit area than any point in the middle of a smooth plane. This effect may be avoided by lowering the wafer into the surface of the substrate holder, to put the substrate surface on the same level as the surface of the surrounding graphite. Neglecting the edge effect, the uniformity of the thickness is better than  $\pm 1\%$ . Fig. 9 illustrates how experimentally, the thickness profile can be adjusted from convex to concave with the ratio of carrier flows, according to the prediction of fig. 8. Fig. 9 also illustrates that the thickness profile is always precisely horizontal, indicating that the wafers turn extremely regularly, without variations of angular velocity within a cycle. This figure also illustrates, how attempts to measure any difference between two wafers grown within the same run have failed so far.

### 5.2. Thin layer structures

An epitaxial layer structure consisting of a series of 6 GaAs quantum wells separated by 1000 Å Ga<sub>0.5</sub>Al<sub>0.5</sub>As barriers was grown. The topmost Ga<sub>0.5</sub>Al<sub>0.5</sub>As layer was also 1000 Å, and a 5000 Å thick Ga<sub>0.5</sub>Al<sub>0.5</sub>As layer separated the first quantum well from the semi-insulating substrate. The substrate orientation was (100) oriented 6° off to (110). The TMG flow during growth of the quantum well was 30 cm³/min at 68 mbar, corresponding to a growth rate on thick layers of 5 Å/s. The arsine flow was 250 cm³/min. The growth temperature was 710°C. The growth times of the quantum wells were 20, 16, 12, 9, 6 and 4 s

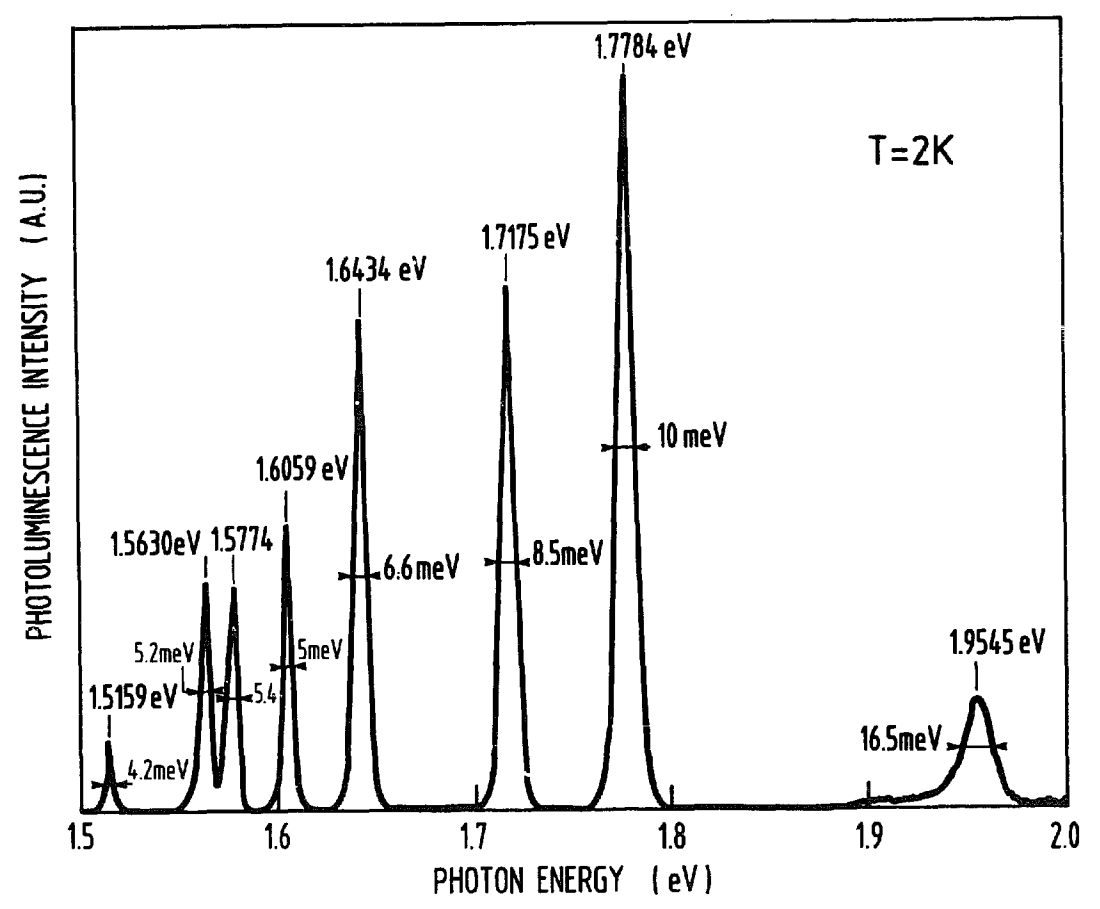


Fig. 10. Photoluminescence spectrum of a series of six GaAs-Ga<sub>0.5</sub>Al<sub>0.5</sub>As quantum wells of different sizes in the same epitaxial layer.

which, according to the steady state growth rate, should give thicknesses of 100, 80, 60, 45, 30 and 20 Å.

Fig. 10 shows the 4 K photoluminescence spectrum of this structure. Using an envelope function

Fig. 11. Layer structure for creation of a highly mobile two-dimensional electron gas.

model [3], the experimental thicknesses calculated from the peak positions are 97.2, 81.1, 62.0, 47.5, 32.2 and 24.8 Å. The thickness of the thinnest

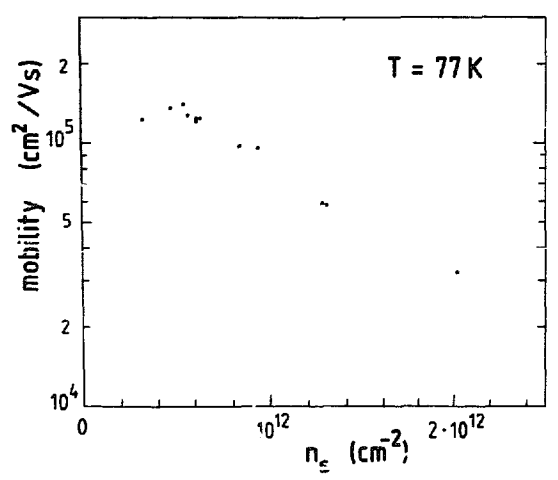


Fig. 12. 77 K Hall mobility versus sheet carrier concentration measured by the Van der Pauw method.

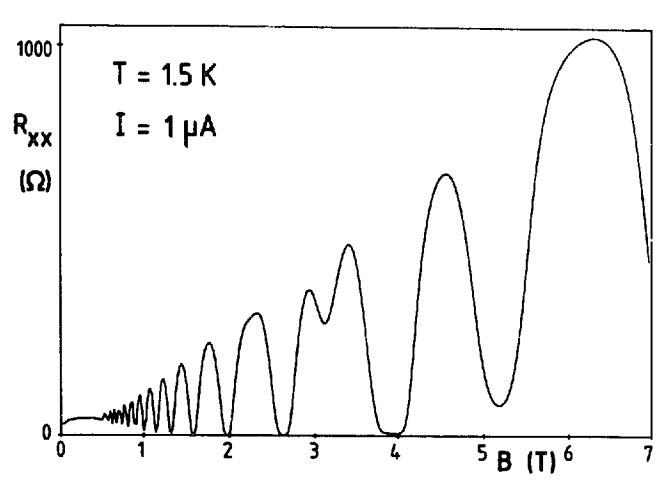


Fig. 13. Shubnikov-De Haas measurement of longitudinal resistivity versus magnetic field. The resulting mobility is 720,000 cm<sup>2</sup>/V·s with a carrier concentration of 3.9×10<sup>11</sup> e/cm<sup>2</sup>.

quantum well appears to follow within the relative error of the measurement (0.3 Å) the thickness profile of fig. 9.

To test the quality of the two-dimensional electron gas obtainable near a GaAs-(Ga,Al)As interface, the structure of fig. 11 was grown many times with different spacer thicknesses. The growth temperature was 680 °C. Fig. 12 shows the 77 K mobility as a function of sheet carrier concentration. A Shubnikov-De Haas measurement has been done (fig. 13) on a sample with a mobility of  $140,000 \text{ cm}^2/\text{V} \cdot \text{s}$  and a carrier density of  $4.0 \times 10^{11} \text{ e/cm}^2$  at 77 K. The sample was cooled down and measured in darkness. This measurement revealed an electron mobility of  $720,000 \text{ cm}^2/\text{V} \cdot \text{s}$  at 1.5 K and a carrier density of  $3.9 \times 10^{11} \text{ e/cm}^2$ .

## 6. Conclusion

A new concept for a MOVPE reactor has been presented. It permits simultaneous epitaxial growth of seven two inch wafers or five 3-inch wafers which evolve in planetary motion around the inner reactor chamber in the form of a ring. The performance of the systems has first been tested on 2 inch wafers at atmospheric pressure using the GaAs-(Ga,Al)As system. Neglecting edge effects, the obtained layers have a thickness uniformity of better than  $\pm 1\%$ , a doping uniformity of better

than  $\pm 1\%$ . The wafer to wafer repeatibility of thickness and doping is better than 1% for all wafers grown in the same run. GaAs-Ga<sub>0.5</sub>Al<sub>0.5</sub>As multiquantum well samples gave intense photoluminescence spectra with FWHM of 5 mV for 100 Å quantum wells and 10 mV for 24 Å quantum wells. Interface quality was further demonstrated by the achievement of a mobility of 720,000 cm<sup>2</sup>/V·s at 1.5 K for a 2D electron gas in a selectively doped GaAs-(Ga,Al)As heterostructure with a sheet carrier concentration of  $3.9 \times 10^{11}$  cm<sup>-3</sup>, which is the highest mobility obtained in an MOVPE grown III-V sample reported to date.

## Acknowledgements

The author would like to thank J.L. Nicolas for his valuable assistance with the fabrication of the reactor, H. Ambrosius for his help and support of the project, and J.N. Patillon and N. Mariel for the Shubnikov-De Haas and optical measurements.

# Notation

Molar concentration
Total molar concentration
Heat capacity at constant pressure
Diffusion constant
Heat transfer coefficient
Total pressure
Gas constant
Temperature
Gas velocity
Kinematic viscosity
· ·
Mass density of gas mixture

# References

- [1] P.M. Frijlink, to be published.
- [2] P.M. Frijlink, A quantitative study of the growth of GaAs and (Ga,Al)As, to be published.
- [3] G. Bastard, ENS Paris, private communication, 1985.